

Article

Microstructure, Phase Composition, and Mechanical Properties of Intermetallic Ni-Al-Cr Material Produced by Dual-Wire Electron-Beam Additive Manufacturing

Elena Astafurova ^{*}, Kseniya Reunova, Elena Zagibalova, Denis Astapov , Sergey Astafurov and Evgenii Kolubaev

Institute of Strength Physics and Materials Science, Siberian Branch of Russian Academy of Sciences, 634055 Tomsk, Russia; reunova.kseniya@ispms.ru (K.R.); zagibalova.elena@ispms.ru (E.Z.); denis.0612@mail.ru (D.A.); svastafurov@ispms.ru (S.A.); eak@ispms.ru (E.K.)

* Correspondence: elena.g.astafurova@ispms.ru

Abstract: Electron-beam additive manufacturing is one of the most promising methods for creating complex metal parts and structures. Additive manufacturing has already gained wide acceptance in the creation of various constructions from aluminum, copper, titanium, and their alloys as well as different classes of steels and other metallic materials. However, there are still many challenges associated with the additive manufacturing and post-production processing of intermetallic alloys. Thus, it is currently an urgent task for research. In this work, heat-resistant intermetallic alloys based on nickel, aluminum, and chromium were produced by dual-wire electron-beam additive manufacturing using commercial NiCr and Al wires. The microstructure, phase composition, and microhardness of the intermetallic billets are strongly dependent on the ratio of NiCr and Al wires, which have been fed during the additive growth of the material (NiCr:Al = 3:1 and NiCr:Al = 1:3). A metal-matrix composite material (Al₃Ni-based intermetallide in Al-based matrix) was fabricated using the NiCr:Al = 1:3 ratio of the wires during the deposition. In tension, it fractures in a brittle manner before the plastic deformation starts, and it possesses a high microhardness of 6–10 GPa with a high dispersion of the value (the mean value is 8.7 GPa). This is associated with the complex phase composition of the material and the high fraction of a brittle Al₃Ni intermetallic phase. In the material, obtained with the ratio NiCr:Al = 3:1, the ordered Ni₃Al(Cr) and disordered Ni₃Cr(Al) intermetallides are the dominating phases. Its microhardness turned out to be lower (4.1 GPa) than that in Al + Al₃Ni-based composite, but intermetallic Ni₃Al-based alloy demonstrates good mechanical properties in a high-temperature deformation regime (650 MPa, more than 10% elongation at 873 K). Microstructural studies, analysis of phase composition, and tensile mechanical properties of additively produced intermetallic materials show the perspective of dual-wire electron-beam additive manufacturing for producing intermetallic compounds for high-temperature applications.

Keywords: electron-beam additive manufacturing; NiCr alloy; Al; intermetallic; microstructure; microhardness; mechanical properties; fracture



Citation: Astafurova, E.; Reunova, K.; Zagibalova, E.; Astapov, D.; Astafurov, S.; Kolubaev, E. Microstructure, Phase Composition, and Mechanical Properties of Intermetallic Ni-Al-Cr Material Produced by Dual-Wire Electron-Beam Additive Manufacturing. *Metals* **2024**, *14*, 75. <https://doi.org/10.3390/met14010075>

Academic Editor: Abdollah Saboori

Received: 28 November 2023

Revised: 22 December 2023

Accepted: 6 January 2024

Published: 8 January 2024



Copyright: © 2024 by the authors. Licensee MDPI, Basel, Switzerland. This article is an open access article distributed under the terms and conditions of the Creative Commons Attribution (CC BY) license (<https://creativecommons.org/licenses/by/4.0/>).

1. Introduction

Currently, additive manufacturing (AM) of metal materials and alloys is one of the most promising ways for the rapid and high-quality creation of products of any shape using a layer-by-layer deposition of materials according to a 3D computer model [1,2].

Unlike the traditional manufacturing of metal materials, the electron-beam-based AM method has several advantages: high efficiency and a high deposition rate, a low cost, and the ability to manufacture products with a complex geometry [1–3]. Today there are several electron-beam 3D printing technologies based on powder bed, wire-feed, and powder-feed systems [1,4–6]. In wire-feed electron-beam additive manufacturing (EBAM), the electron beam is used as a source of energy and a metal wire (or wires) is a feedstock material [1]. The billets (samples, walls) are printed by a layer-by-layer deposition of

the melted feedstock material by an electron beam passing through a magnetic focusing system that forms an ellipse-shaped sweep on the surface of the printing area [1,6]. The density of energy, efficiency, scanning speed, and penetration depth of the electron beam are significantly higher than those of the laser-based AM [1]. During dual-wire EBAM, two wires of different compositions are fed under the electron beam or to the molten pool on the top layer surface of the printing billet. The details of wire-feed EBAM with schemes of wire feeding were previously described in detail in [6].

EBAM is suitable for the fast building of large products, which need a minor finishing post-production treatment [1,6]. In addition, the EBAM process is carried out in a high-vacuum chamber, which prevents materials from oxidation or hydrogenation [1,6]. It is generally believed that additive technologies based on electron-beam methods have several advantages over laser-based methods [1]. They mainly include the ability to obtain pore-free workpieces and the high rate of the additive manufacturing process. However, currently, the first advantage is becoming questionable, as the progressive laser-based additive manufacturing methods allow us to avoid or reduce the formation of macroscopical defects [7]. Regarding the production of intermetallic systems, the problem of cracking the workpieces has remained unsolved, both for electron-beam-based and laser-based methods. It arises not only due to the production peculiarities but also from the brittle nature of the intermetallic systems. Some progress has certainly been made [8–11], but the problem is far from being solved.

The rapid development of the aerospace industry and mechanical engineering requires the creation of materials suitable for operation at high temperatures [12]. Nickel-based superalloys have a high thermal conductivity, high corrosion resistance, and relatively low melting point [12–14]. They are used in gas turbines, jets, and space technologies, where operating temperatures can reach 650–1100 °C [12–15]. Nickel, taken individually, does not have a high elastic modulus, which determines the long-term strength of the material, but the limitations of Ni alloying have a wide range [12,13]. Chromium and aluminum are among the most valuable alloying elements. The solid-solution hardening of nickel by chromium and the high proportion of the γ' -phase (Ni_3Al), when alloying it with aluminum, both provide exceptional mechanical properties for the nickel-based superalloy at elevated temperatures. The Cr and Al oxides, which can form on the surface of the details during operation, can additionally protect the nickel-based alloys from the external aggressive environments, since they are firmly bonded to the matrix and are diffusion-dense [13–16].

Using the arc additive manufacturing method, Meng Y. [17] successfully produced a 3D wall from a Ni-Al alloy. The wall microstructure changed from NiAl/ Ni_3Al to $\text{Ni}_3\text{Al} + \gamma\text{-Ni}/\gamma'\text{-Ni}_3\text{Al}$ with increasing Ni content. The yield strength and the ultimate strength of the additively grown intermetallic compound at room temperature reached 100 MPa and 203 MPa, respectively. The outstanding contribution of the γ' -phase to the strengthening of the γ - γ' systems is determined by the negative temperature dependence of its yield strength and by the activation of latent plasticity, which prevents material from premature fracture [12,18,19]. R.F. Decker and C.G. Bieber established the presence of not only aluminum but also Cr in the γ' -phase of the Inconel 713C alloy [18]. The size of the Cr atoms allows them to occupy the sites of both components of the A_3B compound [1,18]. But for the γ' -phase extracted from the 713C alloy, J. Mihalisin and D. Pasquine demonstrated that most of the chromium atoms are located on the aluminum sublattice; that is, they occupy the right side of the A_3B compound [19]. Thus, chromium, when introduced into a nickel alloy, can increase the volume fraction of the γ' -phase at a given Al content [19]. In other words, alloying a Ni-Al alloy with chromium atoms can increase the γ' -phase content and increase the high-temperature deformability of the compound.

The results of the papers mentioned above demonstrate that additive manufacturing methods are promising techniques for producing intermetallic materials, and they can be used to obtain structurally more complex compositions without the use of rough metallurgical treatments. Methods for producing large workpieces without the formation of

pores and cracks have recently been developed, but the mechanical properties, deformation mechanisms, and fracture of superalloys produced by AM methods have not been fully studied yet [7–9,11,17,20–22]. The aim of this work is to investigate the microstructure, phase composition, and mechanical properties of the intermetallic material produced by dual-wire electron-beam additive manufacturing using commercial NiCr and Al wires.

2. Materials and Methods

Additively manufactured billets with the linear dimensions of $30 \times 35 \times 40 \text{ mm}^3$ were produced by dual-wire electron-beam additive manufacturing (EBAM) using the laboratory equipment and software designed at the Institute of Strength Physics and Materials Science of the Siberian Branch of the Russian Academy of Sciences (ISPMS SB RAS, Tomsk, Russia). During the EBAM process, a two-wire feed of industrially produced NiCr alloy and Al was provided using the scheme previously described in [6]. The chemical compositions of the wires are given in Table 1. The diameter of the wires was 1.2 mm.

Table 1. Chemical composition (in mass. %) of the wires used for the EBAM process.

Wire	Chemical Element											
	Ni	Cr	Al	Fe	C	Si	Mn	S	P	Ti	Cu	Zn
NiCr	73–79	20–23	≤0.2	≤1.5	≤0.1	0.9–1.5	≤0.7	≤0.02	≤0.03	≤0.3	–	–
Al	–	–	≥99.5	≤0.4	–	≤0.3	≤0.05	–	–	≤0.05	≤0.05	≤0.07

During the EBAM process, a sequential deposition of the six parallel tracks of materials was performed in parallel to each other in each layer (a total of 40 layers was deposited in each track and the thickness of the single layer was 0.5–0.7 mm). Two NiCr and Al wires were used simultaneously with the following ratios for the wire feed rates: 1:3 for the “NiCr + 3Al” alloy and 3:1 for the “3NiCr + Al” alloy. The deposition direction changed neither in each layer nor in the next layer. The additive manufacturing process was carried out in a vacuum chamber ($P = 1 \times 10^{-3} \text{ Pa}$) with the following technological parameters: accelerating voltage, 30 kV; beam currents, 15 mA (“NiCr + 3Al” alloy) and 43 mA (“3NiCr + Al” alloy). The $5 \times 5 \text{ mm}$ ellipse-shaped beam with a scanning frequency of 100 Hz was used. The temperature of the billet was not controlled during the EBAM process. The as-built billets were cooled down to 100 °C before air-venting the vacuum chamber to avoid cracking. Austenitic stainless steel (Fe–18%Cr–8%Ni–0.1C, in wt.%) was chosen as a substrate material, and prior to the dual-wire deposition regime, five intermediate NiCr layers were deposited to avoid the influence of the steel composition on the main intermetallic material. The substrate was not cooled during the deposition of the materials to avoid cracking of the intermetallic material due to the thermal stresses [12,13]. Three billets were grown per composition: the “NiCr + 3Al” alloy and the “3NiCr + Al” one. All of the microstructural characterizations and the microhardness were measured in the region of the dual-wire deposition.

Using an electrical discharge machine (DK7750, DQSK, Taizhou City, Jiangsu Province, China), the flat sections were cut from the middle part of the “NiCr + 3Al” and “3NiCr + Al” billets from the normal direction to the deposition direction as shown in the scheme in Figure 1a. Prior to the cutting, sections were etched in an aqua regia. One section per alloy was additionally cut into three types of specimens using an electrical discharge machine: top, center, and bottom specimens (Figure 1b,c). Other sections were used for tensile tests, and the proportional flat dumbbell specimens of $12 \times 2.6 \times 1.2 \text{ mm}^3$ were cut with the tensile axis along the building direction. All samples were mechanically ground and polished using an abrasive paper and aluminum oxide suspension. The samples of the “3NiCr + Al” alloy were additionally electrochemically polished in a solution of chromium anhydride (CrO_3) in phosphoric acid (H_3PO_4) for a final surface purification.

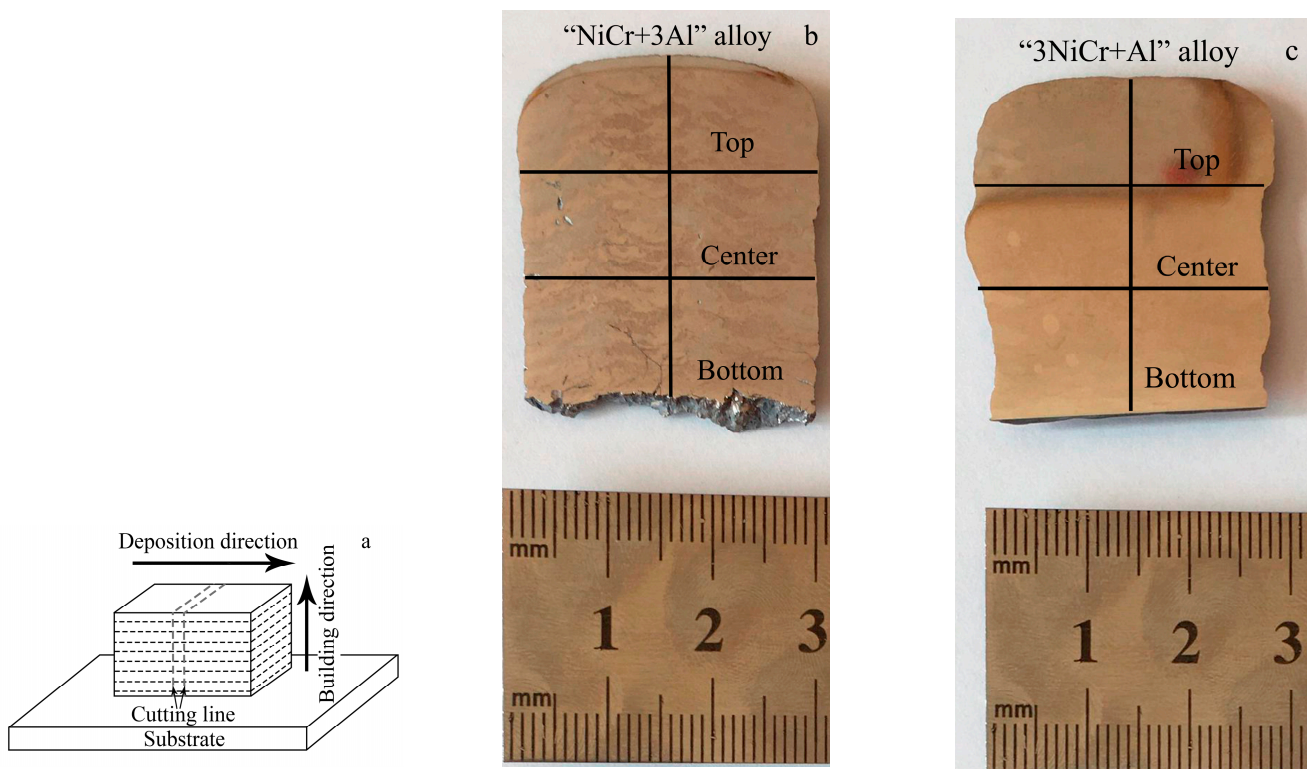


Figure 1. Schematic representation of the intermetallic billet obtained by EBAM, and the position of the sections cut for microstructural analysis (a). The metallographic images of the sections cut from the “NiCr + 3Al” alloy (b) and “3NiCr + Al” alloy (c).

The microstructure of the specimens was investigated using an Altami MET 1C light microscope (Altami, St.-Peterburg, Russia). The phase characterization was conducted by X-ray diffraction (XRD) using a DRON 7 diffractometer (Burevestnik, St. Petersburg, Russia) in the θ -2 θ Bragg-Brentano geometry with a Co-K α radiation. For qualitative phase analysis, the PowderCell program was used to interpret the X-ray diffraction patterns.

A DM8 microhardness tester (AFFRI, Varese, Italy) was used to measure the microhardness by the Vickers method. The load on the indenter was 100 g, and the loading time was 10 s. Vertical lines in the middle of the sections in Figure 1b,c show where the microhardness was measured.

Tension tests were carried out at an initial strain rate of $5 \times 10^{-4} \text{ s}^{-1}$ using an LFM 125 (Walter + Bai AG, Switzerland) electromechanical testing system, and a high-temperature chamber covered the temperature interval from 297 K to 1273 K. Five specimens were tensile tested per each temperature. A force (P) and a displacement of a traverse ($\Delta l = l - l_0$, where l is the length of the deformed sample and l_0 is the initial length of the sample) were collected during each tensile test. These parameters were converted to an engineering stress ($\sigma_e = P/S_0$, S_0 is the initial cross-sectional area of a sample) and an engineering strain ($\epsilon_e = \Delta l/l_0$). The elongation to failure was estimated as the averaged values of $\epsilon_e = \Delta l/l_0$ at failure. Then the true stress ($\sigma_t = \sigma_e (1 + \epsilon_e)$) and true strain ($\epsilon_e = \ln(l/l_0)$) plots were reconstructed, and a yield strength (YS, 0.2% proof stress) and ultimate tensile stress (UTS) were measured using true stress–true strain diagrams.

The microstructure of the initial specimens was investigated using a scanning electron microscope (SEM, Thermo Fisher Scientific Apreo S LoVac, USA), equipped with an energy-dispersive X-ray spectroscopy (EDS) supply.

3. Results and Discussion

Figure 2 shows the microhardness profiles of the intermetallic materials under study. The “NiCr + 3Al” alloy is characterized by an uneven distribution of microhardness along

the length of the workpiece (Figure 2a). The spread of the microhardness values for the “NiCr + 3Al” alloy is high. It takes about 4 GPa, which is almost half of the average value of 8.7 GPa. In the case of the “3NiCr + Al” alloy, the microhardness turned out to be almost two times lower than the mean value typical of the “NiCr + 3Al” alloy (Figure 2b). The alloy is characterized by a relatively uniform distribution of the microhardness value along the entire length of the specimen (Figure 2b). The average value for the 3NiCr + Al alloy is 4.1 GPa, but the microhardness slightly grows moving to the top of the billet.

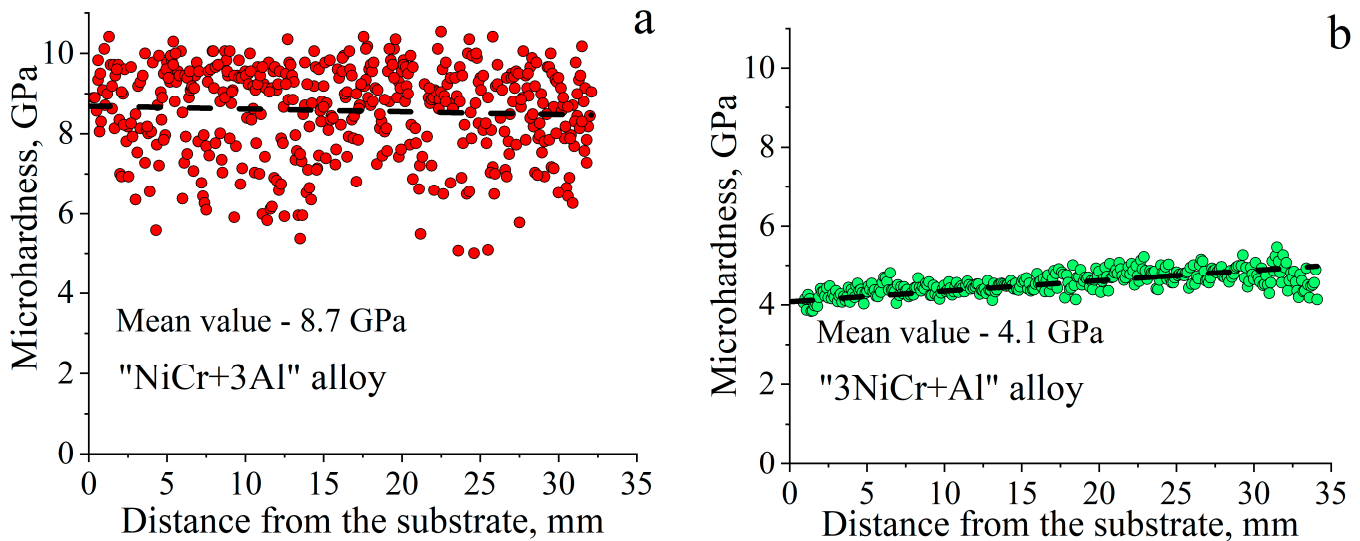


Figure 2. Microhardness profiles in the intermetallic materials under study: (a) “NiCr + 3Al” alloy; (b) “3NiCr + Al” alloy.

The X-ray diffraction patterns obtained for the top, central, and bottom parts of the EBAM-fabricated specimens (the scheme of cutting is shown in Figure 1b,c) are shown in Figure 3. Regardless of the similar composition of the wires used in the EBAM process, different phases were identified in the additively fabricated “NiCr + 3Al” and “3NiCr + Al” alloys. The X-ray diffraction peaks with the highest intensity belong to the phases of Ni_3Cr and Ni_3Al for the “3NiCr + Al” alloy, but Al_3Ni and $\text{Al}(\text{Ni},\text{Cr})$ are characteristic of the “NiCr + 3Al” one. The complex nature of the obtained X-ray diffraction patterns does not allow us to calculate the lattice parameters and volume fractions of the identified phases with high accuracy.

For the “NiCr + 3Al” EBAM-fabricated alloy, the Al_3Ni phase is identified with a high probability because it is determined by a number of XRD lines, and all of them possess high or rather high intensities. The angular position of the strong line left to the (002) Al_3Ni one can be related to alloys on the basis of Al or Ni or the equiatomic NiAl intermetallic phase, but there are no other isolated reflections corresponding to these phases (Figure 3a). So, all of them can be assumed to be like the possible phases.

The $\text{Ni}_3\text{Al}(\text{Cr})$ intermetallic phase, possessing the ordered L_{12} structure [23], is a dominating phase in the “3NiCr + Al” alloy. The appearance of superstructural reflections at small XRD angles is typical of it (for example, (110) Ni_3Al in Figure 3b, bottom pattern). When moving from the bottom to the top of the specimen, the intensity of the superstructural reflections decreases and, in the top part of the specimen, it completely disappears. That is, the process of disordering occurs in the upper part of the billet, and the disordered $\text{Ni}_3\text{Cr}(\text{Al})$ phase becomes the dominating one. In addition to the $\text{Ni}_3(\text{Al},\text{Cr})$, the equiatomic NiAl and pure Al phases are possible but cannot be interpreted with certainty. The XRD lines of these phases are seen in all three parts of the specimen, and the intensity of the single reflection at $2\theta \approx 52^\circ$ remains high.

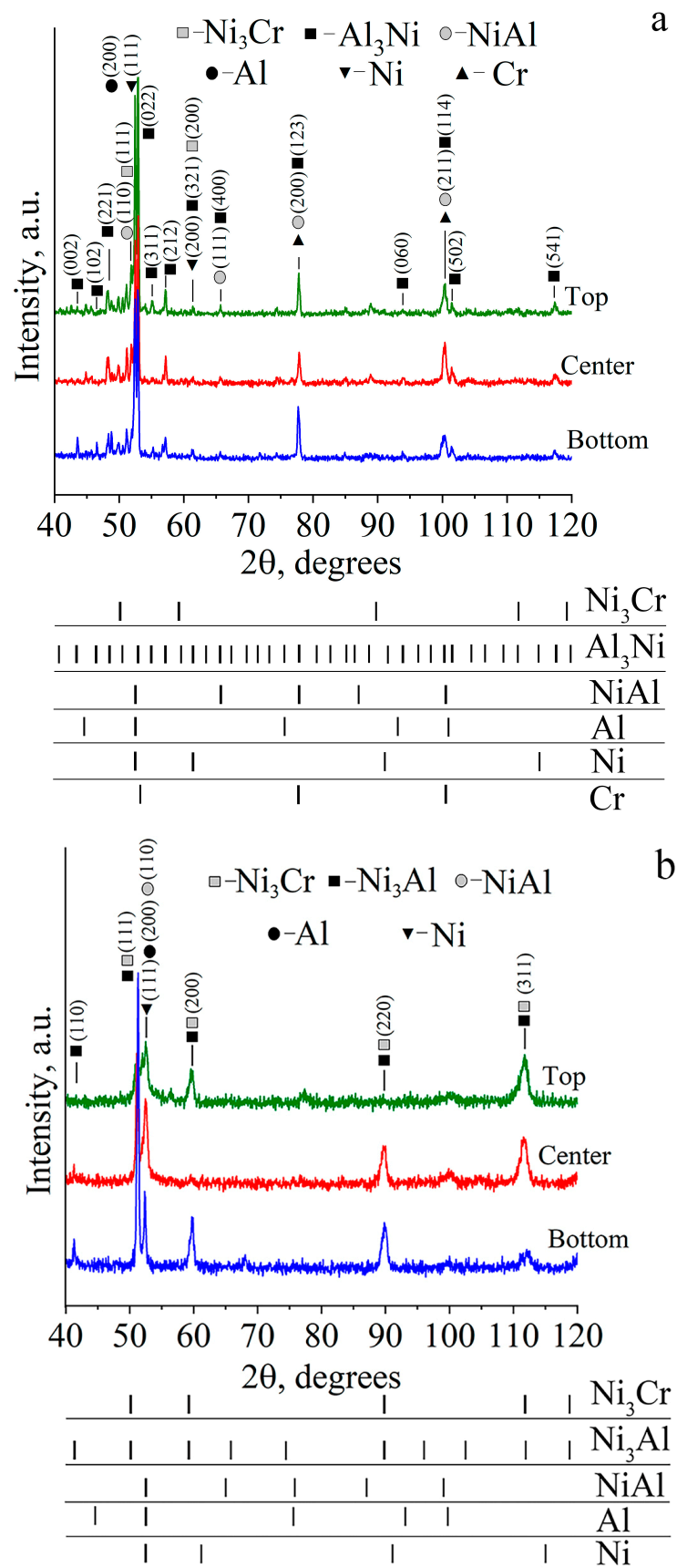


Figure 3. X-ray diffraction patterns of the “NiCr + 3Al” (a) and “3NiCr + Al” (b) specimens of the EBAM-fabricated intermetallic materials.

Figure 4 shows metallographic images of the microstructure in the additively fabricated intermetallic “NiCr + 3Al” and “3NiCr + Al” alloys. The images are intended to reveal the differences between the top, central, and bottom parts of the specimens.

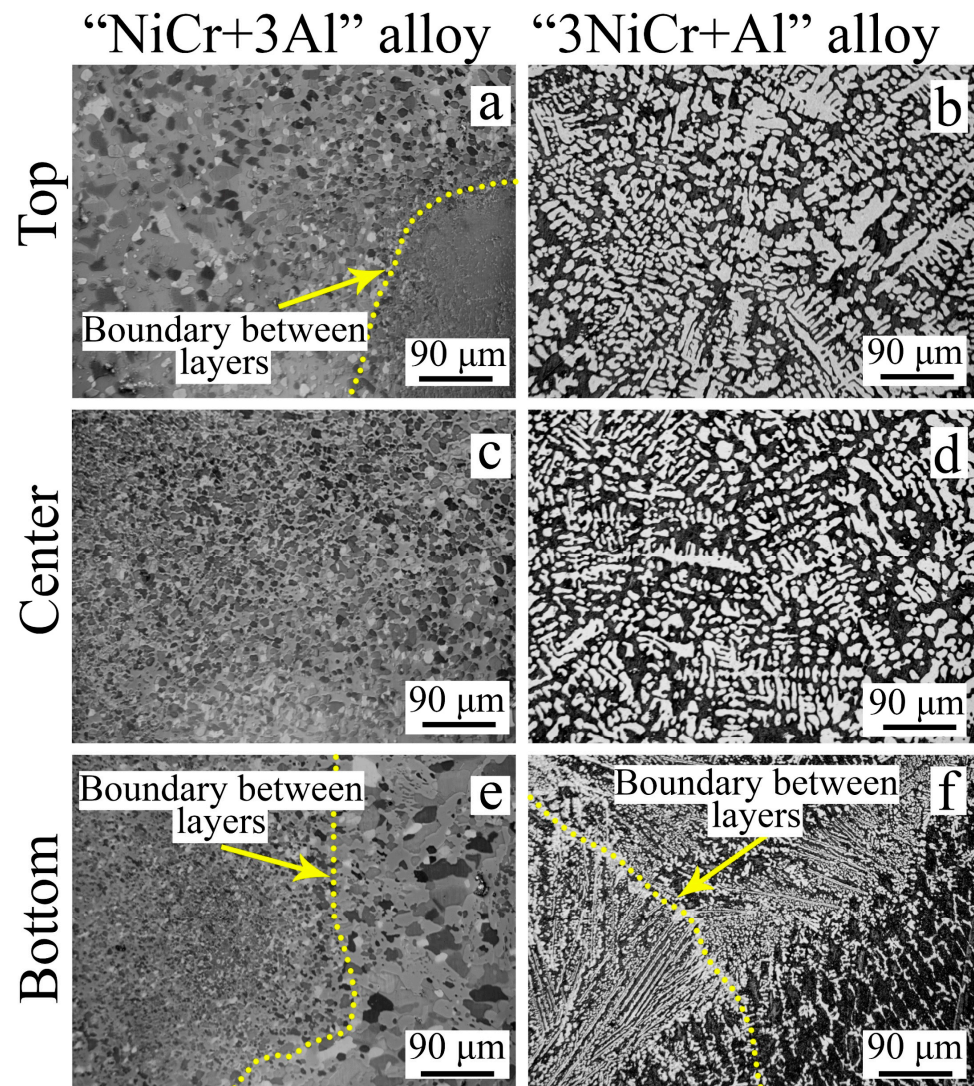


Figure 4. Microstructures of the “NiCr + 3Al” (a,c,e) and “3NiCr + Al” (b,d,f) specimens in the top (a,b), center (c,d), and bottom (e,f) parts of the billets (metallography).

After the EBAM deposition of the materials without post-processing, a macro- and microscopically heterogeneous microstructure is formed in the “NiCr + 3Al” alloy (Figures 1b and 4a,c,e). The macroscopically layered structure is seen on metallographic images (Figure 1b). On the micro-scale, large near-round-shaped grains with $d \approx 70 \mu\text{m}$ are observed in some regions. They are clearly seen in the left part of the image in Figure 4a and the right part of the image in Figure 4e. Along with the coarse-grained polycrystalline structure, the fine-grained polycrystalline regions are observed, in which the mean grain size is $d = 10 \mu\text{m}$ (see, for example, the right part of the image in Figure 4a,c and the left part of the image in Figure 4e). The transition from the coarse-grained to the fine-grained microstructure corresponds to the boundaries between two adjacent layers (shown in Figure 4a,e). Despite the difference in grain sizes, the phase composition of the material is rather homogeneous in different parts of the specimens. Grain-size heterogeneity is typical of additively manufactured materials, and it arises due to the uneven cooling of the layers during AM, which usually provides macroscopically layered materials [1,6]. It is important

to note that the intermetallic alloy does not form columnar grains, which are characteristic of the vast majority of additively manufactured materials [1,6,23]. Consequently, the anisotropy of mechanical properties can be suppressed in the “NiCr + 3Al” intermetallic system. This issue requires further research as part of an independent research work.

Figure 5a shows SEM images of the microstructure in the “NiCr + 3Al” specimen. The data of EDS analysis of the phases are presented in Table 2. In the SEM image, three types of regions with different contrasts are clearly distinguished. The light gray and gray areas represent the Al_3Ni_2 and Al_3Ni phases (Table 2, spectra 1 and 2), and the presence of Al_3Ni was previously confirmed by X-ray diffraction analysis (Figure 3a). The region of a darker shade of gray most likely represents Al alloyed with nickel and chromium (Table 2, spectrum 3). The grains with the composition typical of equiatomic phase NiAl were not revealed during the SEM study of the “NiCr + 3Al” specimen. Considering the limitations of the EDS method for the quantitative measurement of light elements like aluminum, we should rely on the XRD method. Therefore, the phase composition of the “NiCr + 3Al” alloy is mainly presented by the Al_3Ni and Al(Ni,Cr) phases. Due to the complex crystallization processes and thermal history typical of the EBAM process [1,6], the aluminum-enriched phases of the different elemental compositions are formed, which are clearly seen in SEM images by different shades of gray (Figure 5a). As a result, an aluminum matrix composite material has been produced using dual-beam EBAM. The hard intermetallic inclusion of the mainly Al_3Ni phase is incorporated into the rather soft aluminum-based matrix. For this heterophase composite structure, a large scattering of the microhardness is observed. It changes from 5.0 GPa, which is typical of additively-manufactured aluminum alloys [24], to 10.5 GPa, which is characteristic of Al_3Ni intermetallide [25] (Figure 2a).

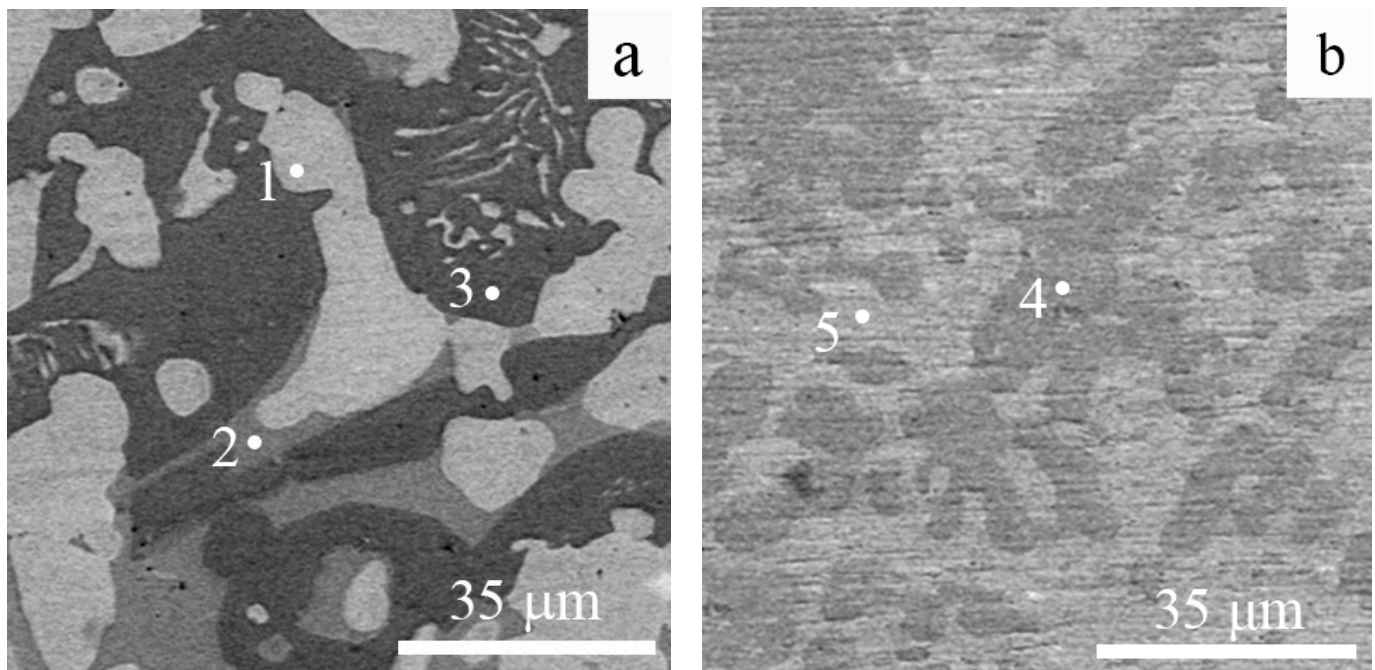


Figure 5. SEM images of the microstructure of the “NiCr + 3Al” (a) and “3NiCr + Al” (b) alloys. The numbers on the figures indicate the points of EDS analysis (the elemental composition is presented in Table 2). SEM images were obtained in the central part of the EBAM-fabricated specimens.

Table 2. EDS data on the elemental composition of the EBAM-fabricated intermetallic alloys and phase composition of the “NiCr + 3Al” and “3NiCr + Al” alloys according to the EDS and X-ray analysis.

Spectrum Number	Ni, at. %	Cr, at. %	Al, at. %	Predicted Phase (EDS)	Predicted Phase (XRD)
“NiCr + 3Al” alloy					
Spectrum 1	38.3	0.6	61.1	AlNi *	
Spectrum 2	24.9	0.5	74.6	Al ₃ Ni or Al ₃ Ni ₂ *	Al ₃ Ni
Spectrum 3	16.4	12.4	71.2	Al(Ni,Cr)	(Al, NiAl-?)
“3NiCr + Al” alloy					
Spectrum 4	60.5	10.4	29.1	Ni ₃ (Al,Cr) or NiAl *	Ni ₃ Al, Ni ₃ Cr
Spectrum 5	61.4	25.9	12.7	Ni ₃ (Cr,Al) or Ni(Cr,Al) + Ni ₃ (Cr,Al) *	(Ni, NiAl-?)

* Assuming that the aluminum content is overestimated and moving to the right in the binary phase diagram of Ni-Al [14].

Another microstructure was previously reported by I.V. Shishkovsky when he tried to form a gradient-layered material by laser cladding using a mixture of NiCr and Al powders [26]. In the region, where a 30%NiCr + 70%Al powder mixture was used for additive manufacturing, there were needle-like microstructures with impregnations of intermetallic phases (NiCr matrix with NiAl and AlCr₂ phases). The microhardness varied in the interval of 520–780HV_{0.1}. This interval lies in the microhardness interval in Figure 2a, but its nature is different because of the difference in phase compositions and the morphology of the structure in the materials reported in [26] and the “NiCr + 3Al” material. Therefore, despite the close ratio of the components (NiCr and Al), the additive manufacturing methods and regimes are very important issues.

In the “3NiCr + Al” alloy, the microstructure under study is rather homogeneous with dendritic segregations (Figure 4b,d,f). The morphology of dendrites is similar for the top, central, and upper parts of the specimen, but the dendritic arms are thinner and longer in the lower part of the billet due to the higher cooling rate at the beginning of the EBAM process [1,6]. Two characteristic phases of Ni₃Al and Ni₃Cr were identified by XRD analysis with high accuracy, and the possible formation of NiAl was detected (Figure 3b). According to the EDS analysis, the dendritic phase is enriched by Ni and Al (Figure 5b, Table 2) and can be in both the Ni₃(Al,Cr) or NiAl phases assuming the Al content is overestimated in the EDS analysis. The detected phases in the interdendritic regions are most likely intermetallic Ni₃Cr-based phases or mixtures of Ni(Cr,Al) + Ni₃(Cr,Al). Some of the Al and Cr atoms are substituted by Cr and Al, respectively, in the Ni₃Cr-based phases. The SEM EDS data correlate well with the results of the X-ray diffraction analysis of the alloy (Figures 3b and 5b, Table 2). So, the “3NiCr + Al” specimen is an intermetallic alloy with a complex composition based on the Ni₃Al phase.

The microhardness of the “3NiCr + Al” alloy is slightly above 4GPa, which is very close to the values reported previously for the bulk Ni₃Al and NiAl alloys: about 450 HV_{0.3} for the NiAl + Ni₃Al alloy and about 300 HV_{0.3} for the γ -Ni + γ' -Ni₃Al one [17]. As the alloy is macroscopically homogeneous, the microhardness changes insignificantly along the as-fabricated billet, and the scattering of the values is low relative to the “NiCr + 3Al” alloy (Figure 2b). As microstructure changes insignificantly along the AM-fabricated billet, this change in microhardness is associated with the variation in the elemental composition of the main phase. Moving to the top of the “3NiCr + Al” specimen, the fraction of the ordered phase Ni₃(Al,Cr) decreases, and contrarily, the fraction of the disordered Ni₃Cr(Al) phase increases. Two phases, Ni₃(Al,Cr) and Ni₃Cr(Al), are Ni₃Al-based phases, which are slightly different in elemental composition (in one of them the concentration of chromium prevails and the concentration of aluminum is higher in the other), but the Ni₃(Al,Cr) is the ordered phase. Due to the similar nature of both phases, the scattering of the microhardness is low, and the microhardness variation along the billet height is insignificant but visible. The microhardness of the “3NiCr + Al” alloy is two times lower than that of the “NiCr +

3Al” alloy, which is due to the absence of the hard and brittle Al_3Ni phase in the “3NiCr + Al” specimens.

Figures 6 and 7 show the tensile diagrams in engineering coordinates and the temperature dependencies of the main mechanical properties of the “3NiCr + Al” alloy. The plasticity of the alloy is limited at a low-temperature deformation regime, but at temperatures higher than 673 K, the specimens show good elongations (Figure 7a). The best combination of strength and plasticity is achieved at the temperature of 873 K (Figures 6 and 7).

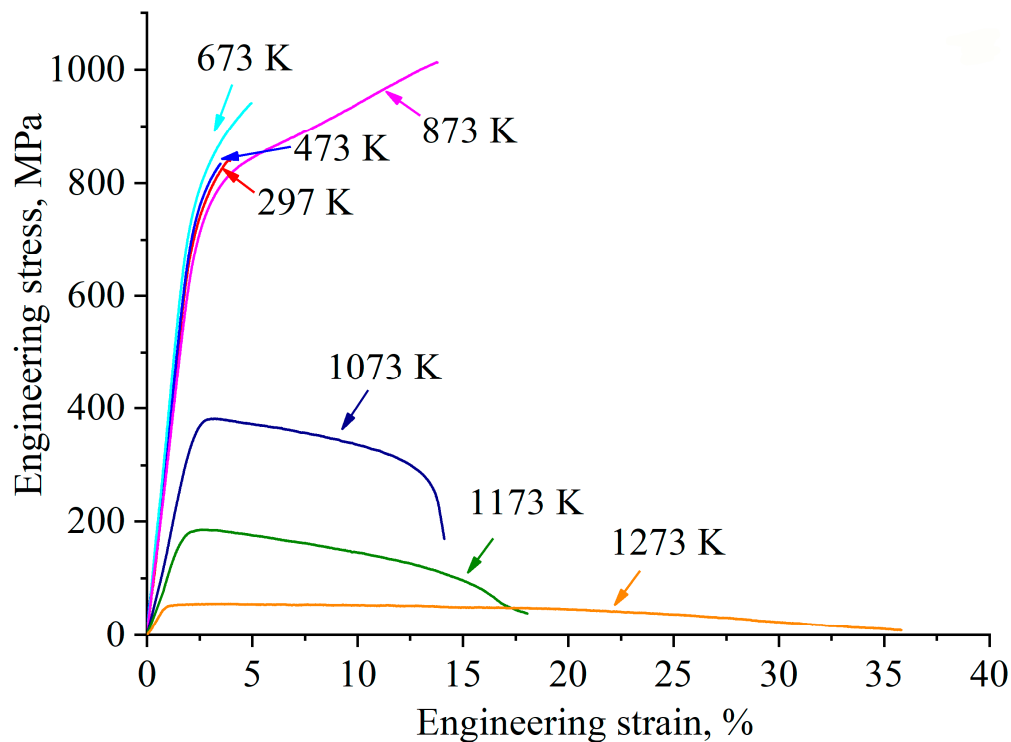


Figure 6. Tensile “engineering stress-engineering strain” diagrams of the “3NiCr + Al” EBAM-fabricated alloy.

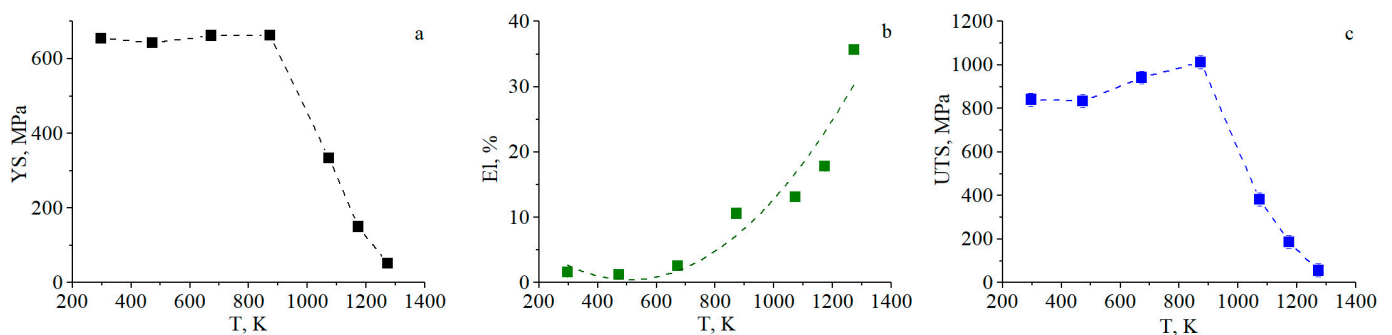


Figure 7. The temperature dependence of the yield strength (YS) (a), elongation-to-failure (EL) (b), and ultimate tensile stress (UTS) (c) of the “3NiCr + Al” EBAM-fabricated alloy.

The value of the yield strength (YS) changes slightly (about 650 MPa) in the temperature range from 297 K to 873 K (Figure 7a). High mechanical properties at $T \leq 873$ K are associated with a solid-solution strengthening of the γ' - Ni_3Al phase by chromium [27].

The increased flow stress with increasing temperature is called anomalous strengthening and is a significant property of the plastic deformation of intermetallic compounds [28]. The mechanisms for the anomalous plastic behavior of L_2 compounds like Ni_3Al are based on the role of the dislocation core configurations (superdislocations in ordered crystal struc-

tures) and operating slip systems. This mechanism was widely accepted in most research works and described by the authors of [28]. A further increase in the test temperature to 1273 K is accompanied by a normal temperature dependence of the YS, so the YS is just 52 MPa at $T = 1273$ K (Figure 7a). The temperature dependence of the ultimate tensile stress (UTS) demonstrates behavior similar to the YS: the “3NiCr + Al” alloy is characterized by high strength properties in the temperature range from 297 K to 873 K (Figure 7c). Therefore, additively fabricated intermetallic compounds show perspective mechanical properties for high-temperature applications.

It should be noted that the study of tensile properties was not carried out for the “NiCr + 3Al” alloy due to the premature fracture of the specimens during loading or even during specimens’ polishing, which is due to the brittle Al_3Ni phase [29].

4. Conclusions

In the present paper, we investigated the microstructure, phase composition, microhardness, and mechanical properties of the intermetallic materials fabricated using wire-feed electron-beam additive manufacturing with deposition of industrial NiCr and Al wires (the ratios of NiCr and Al varied from 1:3 to 3:1). The main results can be summarized as follows:

1. A macro- and microscopically heterogeneous microstructure is formed in the “NiCr + 3Al” alloy fabricated with a ratio of the wires of NiCr:Al = 1:3. Microstructural analysis shows that the aluminum matrix composite material has been produced using dual-beam EBAM. The phase composition of the “NiCr + 3Al” alloy is mainly presented by the Al_3Ni and $\text{Al}(\text{Ni},\text{Cr})$ phases and is independent of the position in the as-received billet. The macroscopically layered structure forms due to the microscopic heterogeneities of the grain structure. At the micro-scale, the regions of the coarse-grained and those of the fine-grained polycrystalline structure form during the EBAM process. This composite structure possesses high microhardness (the mean value is 8.7 GPa), but the specimens are too brittle for any tensile tests due to the presence of the Al_3Ni intermetallic phase.
2. The EBAM-fabricated “3NiCr + Al” alloy (the wire ratio is NiCr:Al = 3:1) possesses a homogeneous dendritic microstructure on the base of two phases of Ni_3Al and Ni_3Cr . The microhardness of the “3NiCr + Al” alloy is slightly above 4 GPa, which is two times lower than that of the “NiCr + 3Al” aluminum matrix composite material. Despite this, the “3NiCr + Al” alloy shows a good combination of tensile properties, with the best combination of strength and plasticity at a temperature of 873 K (650 MPa, more than 10% elongation). The anomalous temperature dependence of the yield strength was observed for this alloy in the temperature interval (300–873) K, which is the significant property of the plastic deformation of the intermetallic compounds.

Thus, the two-wire EBAM process is a suitable technology for prototyping intermetallic alloys for high-temperature applications. The EBAM technology used in this work for the AM of the intermetallic alloy based on industrial NiCr and Al wires has the limitation of the size of the workpiece, which is limited by the size of the vacuum chamber (which can reach several meters). It is also necessary to take into account the possible anisotropy of the properties in the resulting intermetallic billet, which has not been studied in this work.

Author Contributions: Conceptualization, E.A. and E.K.; methodology, S.A. and E.A.; investigation, K.R., D.A., E.Z. and S.A.; data curation, K.R., E.Z. and D.A.; writing—original draft preparation K.R., E.Z. and D.A.; writing—review and editing E.A. and E.K.; visualization, K.R. and E.Z.; supervision, E.A. and E.K.; project administration, E.A. and E.K.; funding acquisition, E.A. and E.K. All authors have read and agreed to the published version of the manuscript.

Funding: This research was funded by the Government research assignment for ISPMS SB RAS, project FWRW-2022-0005.

Data Availability Statement: The data are available on request.

Acknowledgments: The investigations were conducted using the equipment of the Institute of Strength Physics and Materials Science (“Nanotech” center). The authors thank V. Rubtsov and S. Nikonov for their assistance with the additive manufacturing of the material.

Conflicts of Interest: The authors declare no conflicts of interest.

References

1. Frazier, W.E. Metal Additive Manufacturing: A Review. *J. Mater. Eng. Perform.* **2014**, *23*, 1917–1928. [CrossRef]
2. Cunningham, C.R.; Flynn, J.M.; Shokrani, A.; Dhokia, V.; Newman, S.T. Invited review article: Strategies and processes for high quality wire arc additive manufacturing. *Addit. Manuf.* **2018**, *22*, 672–686. [CrossRef]
3. Song, B.; Dong, S.; Coddet, P.; Liao, H.; Coddet, C. Fabrication of NiCr alloy parts by selective laser melting: Columnar microstructure and anisotropic mechanical behavior. *Mater. Des.* **2014**, *53*, 1–7. [CrossRef]
4. Ding, D.; Pan, Z.; Cuiuri, D.; Li, H. Wire-feed additive manufacturing of metal components: Technologies, developments, and future interests. *Int. J. Adv. Manuf. Technol.* **2015**, *81*, 465–481. [CrossRef]
5. Utela, B.; Storti, D.; Anderson, R.; Ganter, M. A review of process development steps for new material systems in three-dimensional printing (3DP). *J. Manuf. Process.* **2008**, *10*, 96–104. [CrossRef]
6. Kolubaev, E.A.; Rubtsov, V.E.; Chemaevsky, A.V.; Astafurova, E.G. Micro-, meso- and microstructural design of bulk metallic and polymetallic materials by wire-feed electron-beam additive manufacturing. *Phys. Mesomech.* **2022**, *25*, 479–491. [CrossRef]
7. Wang, Y.; Guo, W.; Xie, Y.; Li, H.; Zeng, C.; Xu, M.; Zhang, H. In-situ monitoring plume, spattering behavior and revealing their relationship with melt flow in laser powder bed fusion of nickel-based superalloy. *J. Mater. Sci. Technol.* **2024**, *177*, 44–58. [CrossRef]
8. Park, J.-U.; Jun, S.-Y.; Lee, B.H.; Jang, J.H.; Lee, B.-S.; Lee, H.-J.; Lee, J.-H.; Hong, H.-U. Alloy design of Ni-based superalloy with high γ' volume fraction suitable for additive manufacturing and its deformation behavior. *Addit. Manuf.* **2022**, *52*, 102680. [CrossRef]
9. Wei, B.; Liu, Z.; Cao, B.; Nong, B.; Zhang, Y.; Zhou, H.; Ai, Y. Selective laser melting of crack-free Rene 104 superalloy by Sc microalloying. *J. Alloys Compd.* **2022**, *895*, 162663. [CrossRef]
10. Harrison, N.J.; Todd, I.; Mumtaz, K. Reduction of micro-cracking in nickel superalloys processed by selective laser melting: A fundamental alloy design approach. *Acta Mater.* **2015**, *94*, 59–68. [CrossRef]
11. Gurianov, D.A.; Fortuna, S.V.; Nikonov, S.Y.; Vorontsov, A.V. Influence of additive process parameters on formation of superalloy product structure. *AIP Conf. Proc.* **2020**, *2310*, 020121.
12. Sims, T.; Stoloff, S.; Hagel, C. *Superalloys II: High-Temperature Materials for Aerospace and Industrial Power*; Wiley-Interscience: Hoboken, NJ, USA, 1987; 640p.
13. Smialek, J. *Microstructure of Al₂O₃ Scales Formed on NiCrAl Alloys*; NASA: Washington, DC, USA, 1981; p. 33.
14. Ramandhany, S.; Sugiarti, E.; Desiati, R.; Martides, E.; Junianto, E.; Prawara, B.; Sukarto, A. The effect of silicon as a reactive element for NiCrAl coating performance on hastelloy substrate. *IOP Conf. Ser. Mater. Sci. Eng.* **2018**, *432*, 012017. [CrossRef]
15. Yancheshmeh, D.; Esmailian, M.; Shirvani, K. Microstructural and oxidation behavior of NiCrAl super alloy containing hafnium at high temperature. *Int. J. Hydrog. Energy* **2018**, *43*, 5365–5373. [CrossRef]
16. Zhen, H.; Xie, Y.; Tian, L.; Peng, X. Discontinuous oxidation in wet air of T91 with a novel Al₂O₃-forming NiCrAl nanocomposite coating in as-deposited and pre-oxidized states. *Surf. Coat. Technol.* **2022**, *449*, 128937. [CrossRef]
17. Meng, Y.; Li, J.; Gao, M.; Zeng, X. Microstructure characteristics of wire arc additive manufactured Ni-Al intermetallic compounds. *J. Manuf. Process.* **2021**, *68*, 932–939. [CrossRef]
18. *STP245-EB*; Symposium on Electron Metallography. ASTM International: West Conshohocken, PA, USA, 1966; p. 262.
19. Mihalisin, J.; Pasquine, D. Phase Transformation in Nickel-Base Alloys. In Proceedings of the International Symposium on Structural Stability in Superalloys, Seven Springs, Champion, PA, USA, 4–6 September 1968; pp. 134–170. Available online: https://www.tms.org/superalloys/10.7449/1968/Superalloys_1968_134_170.pdf (accessed on 27 November 2023).
20. Reunova, K.A.; Zagibalova, E.A.; Astapov, D.O.; Astafurov, S.V.; Kolubaev, E.A.; Astafurova, E.G. Microstructure, Phase Composition, and Microhardness of the NiCr/Al Gradient Material Produced by Wire-Feed Electron-Beam Additive Manufacturing. *Russ. Phys. J.* **2023**, *66*, 341–349. [CrossRef]
21. Gurianov, D.A.; Fortuna, S.V.; Nikonov, S.Y.; Moskvichev, E.N.; Kolubaev, E.A.; Rubtsov, V.E.; Sokolov, P.S. Characterization of Microsegregation and Secondary Phase Precipitation in Nickel-Based Superalloy after Wire-Feed Electron Beam Additive Manufacturing. *Russ. Phys. J.* **2022**, *65*, 1396–1403. [CrossRef]
22. Wang, J.; Wang, H.; Gao, H.; Deng, H.; Zhang, M.; Cheng, X.; Zhang, S.; Liu, D. Origin of hot cracking formation and suppression method in laser additive manufactured nickel-based superalloys. *Mater. Lett.* **2023**, *352*, 135200. [CrossRef]
23. Melnikov, E.V.; Astafurova, E.G.; Astafurov, S.V.; Maier, G.G.; Moskvina, V.A.; Panchenko, M.Y.; Fortuna, S.V.; Rubtsov, V.E.; Kolubaev, E.A. Anisotropy of the tensile properties in austenitic stainless steel obtained by wire-feed electron beam additive growth. *Lett. Mater.* **2019**, *9*, 460–464. [CrossRef]
24. Guo, N.; Cheng, Q.; Fu, Y.; Gao, Y.; Chen, H.; Zhang, S.; Zhang, X.; He, J. Microstructure and microhardness of aluminum alloy with underwater and in-air wire-feed laser deposition. *Int. J. Miner. Metall. Mater.* **2023**, *30*, 670–677. [CrossRef]

25. Op, A.R.N.; Arul, S. Effect of Nickel reinforcement on micro hardness and wear resistance of aluminium alloy Al7075. *Mater. Today Proc.* **2020**, *24*, 1042–1051.
26. Shishkovsky, I.V. Laser controlled intermetallics synthesis during surface cladding. In *Laser Surface Engineering*; Woodhead Publishing: Sawston, UK, 2015; pp. 237–286.
27. Povarova, K.B.; Bazyleva, O.A.; Drozdov, A.A.; Kazanskaya, N.K.; Morozov, A.E.; Samaonova, M.A. Structural heat-resistant alloys based on Ni₃Al: Preparation, structure and properties. *Mater. Sci.* **2011**, *4*, 39–48.
28. Zhang, J.S. *High Temperature Deformation and Fracture of Materials*; Woodhead Publishing: Sawston, UK, 2010.
29. Balakrishnan, M.; Dinaharan, I.; Kalaiselvan, K.; Palanivel, R. Friction stir processing of Al₃Ni intermetallic particulate reinforced cast aluminum matrix composites: Microstructure and tensile properties. *J. Mater. Res. Technol.* **2022**, *9*, 4356–4367. [[CrossRef](#)]

Disclaimer/Publisher’s Note: The statements, opinions and data contained in all publications are solely those of the individual author(s) and contributor(s) and not of MDPI and/or the editor(s). MDPI and/or the editor(s) disclaim responsibility for any injury to people or property resulting from any ideas, methods, instructions or products referred to in the content.